Net Acceleration and Direct Measurement of Attosecond Electron Pulses in a Silicon Dielectric Laser Accelerator

Dylan S. Black,[1] Uwe Niedermayer,[3] Yu Miao,[1] Zhexin Zhao,[1] Olav Solgaard,[1] Robert L. Byer,[2] and Kenneth J. Leedle[1]
[1]Department of Electrical Engineering, Stanford University, 350 Serra Mall, Stanford, California 94305-9505, USA
[2]Department of Applied Physics, Stanford University, 348 Via Pueblo Mall, Stanford, California 94305-4090, USA
[3]Technische Universität Darmstadt, Institut für Teilchenbeschleunigung und Elektromagnetische Felder (TEMF), Schloßgartenstr. 8, 64289 Darmstadt, Germany

(Received 25 June 2019; revised manuscript received 3 August 2019; published 26 December 2019)

Net acceleration of attosecond-scale electron pulses is critical to the development of on-chip accelerators. We demonstrate a silicon-based laser-driven two-stage accelerator as an injector stage prototype for a Dielectric Laser Accelerator (DLA). The first stage converts a 57-keV (500 ± 100)-fs (FWHM) electron pulse into a pulse train of 700 ± 200 as (FWHM) microbunches. The second stage harnesses the tunability of dual-drive DLA to perform both a net acceleration and a streaking measurement. In the acceleration mode, the second stage increases the net energy of the electron pulse by 200 eV over 12.25 μm. In the deflection mode, the microbunch temporal profile is analyzed by a direct streaking measurement with 200 as resolution. This work provides a demonstration of a novel, on-chip method to access the attosecond regime, opening new paths towards attosecond science using DLA.

DOI: 10.1103/PhysRevLett.123.264802

Combining the GV/m fields of femtosecond lasers with the high damage thresholds of dielectric materials and the nanofabrication expertise of the semiconductor industry has enabled construction of the highest-gradient nonplasma particle accelerators that currently exist [1]. However, previous demonstrations of Dielectric Laser Accelerators (DLAs) [2,3] have almost exclusively performed energy *modulation* experiments, with equal numbers of accelerated and decelerated particles. Net acceleration requires bunch compression to a fraction of an optical cycle, similar to conventional radio frequency injector stages [4,5]. A DLA injector which can achieve net acceleration with femtosecond optical cycles must therefore produce attosecond-scale bunches.

Attosecond electron pulses are the subject of recent pioneering research [6–11]. For example, ultrafast electron diffraction (UED) uses ultrashort electron pulses to resolve molecular dynamics on femtosecond time scales [12–14]. Attosecond-scale UED would allow sufficient resolution to resolve intramolecular electronic dynamics. Attosecond-scale electron pulses could also provide superradiant enhancement to Smith-Purcell radiators for wavelengths in the VUV-XUV range [15].

Recently, microbunched pulse trains using dielectric structures have been investigated in the THz regime, using charge-dependent self-modulation to achieve microbunching [16]. Laser-driven attosecond-scale microbunching of relativistic electron beams has also been achieved in an inverse free-electron laser, using a magnetic chicane as the dispersive element [17]. However, in a fully on-chip DLA injector, it is simpler to use a velocity bunching scheme while the beam is subrelativistic [18,19].

In this Letter, we generate attosecond-scale microbunched pulse trains by velocity bunching in a subrelativistic, on-chip DLA. We inject this pulse train into a second DLA stage at a tunable injection phase, and observe net acceleration by 200 eV over 12.25 μm. By tuning the optical mode of the second stage, we characterize the microbunch duration by a direct streaking measurement with an estimated temporal resolution of 200 as. The microbunches produced are measured to be as short as 700 ± 200 as FWHM. The streaking resolution achieved is on par with state-of-the-art direct measurement techniques (~100 as resolution) [20–23].

The theory of dual-drive DLA is detailed in [24–26]. We choose a coordinate system $(x, x', y, y', \varphi \equiv \omega\Delta t, E)$, where x and y are the transverse offsets from the beam axis (z) passing through the center of the pillars, x' and y' are the corresponding trajectory angles relative to the z axis, φ is the longitudinal injection phase of an electron relative to the laser field in the structure, Δt is the time delay of an electron relative to a reference particle, ω is the laser angular frequency, and E is the electron energy.

The dual-drive DLA has symmetric and antisymmetric modes, determined by the relative (dual-drive) laser phase: $\theta_1 - \theta_2 = 0, \pm\pi$ for symmetric and antisymmetric modes, respectively [Fig. 1(a)]. In the symmetric mode, the energy gain of a phase-matched particle over N periods of length Λ is

$$\Delta E = -qe_1 N\Lambda \cosh\left(\frac{\omega}{\beta c\gamma} y\right) \cos\omega\Delta t, \qquad (1)$$

where β is the normalized electron velocity v_e/c, $\gamma = (1-\beta^2)^{-1/2}$, and e_1 is defined as the synchronous on axis accelerating field [24]. Experimentally, e_1 is measured by observation of the accelerating gradient of the on axis electrons, visible as the peak of the double-horns energy spectrum (see the Supplemental Material [27]). For clarity, we define the elementary charge q to be 1 and quote all measurements of e_1 in units of MeV/m.

The electron bunch energy is modulated according to Eq. (1) by the first DLA stage. Electrons with injection phase $\omega\Delta t \in [-(\pi/2), (\pi/2)]$ lose energy, and electrons with $\omega\Delta t \in [(\pi/2), (3\pi/2)]$ gain energy. For on axis particles, the faster electrons intersect the slower ones after a distance f_t to create maximally short microbunches spaced by one optical period (Fig. 1). In the limit of linear chirp,

$$f_t \approx \frac{m_e c^2 \beta^2 \gamma^3}{\zeta q e_1 N}, \tag{2}$$

where m_e is the electron mass, and $\zeta = 2\pi$ if the intrinsic energy spread limits the microbunch duration [29]. If the energy spread is negligible, $\zeta = 4$ [19]. When $\zeta = 2\pi$, this "temporal focal length" is equal to the spatial focal length of a DLA lens [30].

In the antisymmetric mode, the particle angular deflection $\Delta y'$ over N periods is

$$\Delta y' \approx \frac{q e_1 N \Lambda}{\beta^2 \gamma^2 m_e c^2} \sin \omega\Delta t, \tag{3}$$

see Ref. [30].

The antisymmetric mode allows direct measurement of the average microbunch duration within the pulse train. In this mode, the deflection force is proportional to $\sin \omega\Delta t$ [Eq. (3)]. When $\omega\Delta t$ is small, the deflection angle has a linear dependence on the electron time delay given by

$$\Delta y' \approx D\Delta t, \tag{4}$$

where D (mrad/fs) is the "streaking speed" [20] or "shear parameter". The time delay Δt of an electron entering an antisymmetric-mode DLA is therefore linearly mapped onto $\Delta y'$ in the linear region of the laser field.

The electron beam has intrinsic divergence derived from its emittance—in a streaking measurement, the duration of the microbunch manifests as a broadening of the intrinsic deflection spectrum. The microbunch temporal profile can be recovered by deconvolving the lasers-on (streaked) bunch profile with the lasers-off (unstreaked) profile.

DLATrack6D simulations [24] predict that for intrinsic energy spreads < 1 eV, single-digit attosecond bunches occur exactly at the longitudinal focus, but rapidly broaden with larger energy spreads. For energy spread dominated beams, microbunch duration scales approximately linearly with energy spread [29].

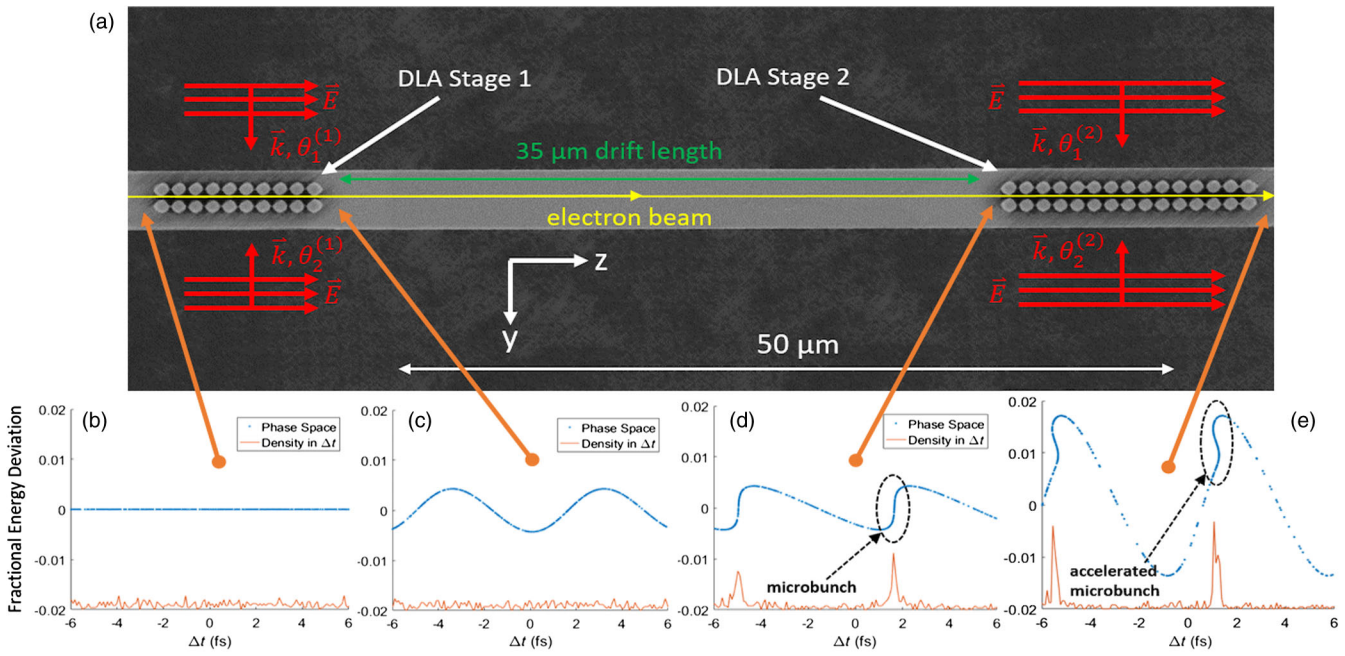

FIG. 1. (a) An electron beam travels through two DLA stages separated by a 35 μm drift length, each driven by two laser pulses. All four pulses are identical and phase locked, with phases given by $\theta_1^{(1)}, \theta_2^{(1)}$ and $\theta_1^{(2)}, \theta_2^{(2)}$. (b) An example particle distribution with average kinetic energy 57 keV. The electron density is initially uniform over Δt. (c) The bunching stage modulates the electron energy. (d) The drift shears the phase space and modulates the electron density. Pulse train formation by microbunching is visible. (e) The pulse train is injected into an accelerating stage, and its net energy increases.

The energy spread produced by the bunching stage causes significant microbunch evolution over the length of the streaker. The recovered temporal profiles should therefore be understood as the *average* microbunched pulse train profile over the length of the streaker. The recovered microbunch duration is not strongly affected by the minimum bunch duration for durations below ~200 as FWHM, instead being dominated by the bunch evolution.

Two stages of dual-pillar DLAs like those in [26,30] are fabricated from monolithic 5–10 Ω cm B:Si (Fig. 1). Pairs of elliptical pillars 2.7 μm in height with a channel gap of 300 nm are spaced by a periodicity Λ of 875 nm. The first DLA stage has ten pillars (thus nine active periods, length 7.88 μm) followed by a 35 μm drift length, then a second DLA stage with fifteen pillars (14 periods, 12.25 μm length) (Fig. 1).

A fraction of a 1 μm, 100 kHz, 300 fs regenerative amplifier pulse is used to generate the initial 500 ± 100 fs FWHM electron pulse from a silicon nanotip photocathode [31]. It has a central energy of 57 keV and energy spread < 10 eV. The electron pulse is focused to a 120 ± 25 nm RMS spot at the DLA, and its divergence is set to 1 mrad half-angle by an aperture, giving a geometric emittance of 120 ± 25 pm-rad. Electron currents of $< 1e^-$/pulse (at the cathode) ensure that space-charge-induced temporal broadening is minimal. Electron current at the DLA is limited by the aperture to roughly 1000 e^-/s. Beam transmission through the DLA is further limited by suboptimal matching to the transverse structure acceptance [32]. The transmitted current is approximately 300 e^-/s (30%).

The remainder of the regenerative amplifier pulse pumps an OPA which generates a 1980 nm, 605 ± 5 fs pulse. This pulse is split into four accelerator drive pulses—two per stage (Fig. 1). Each identical drive pulse, having energy between 20 and 45 nJ depending on the desired e_1, is focused to a $1/e^2$ radius of 20 ± 1 μm.

The first accelerator stage is operated in the symmetric mode, which produces a microbunched pulse train at the second stage. The temporal focal length of the first stage is matched to the drift length between stages (35 μm) for $e_1 = 60$ MeV/m. The second stage is operated in symmetric mode for net acceleration (Fig. 2), or tuned to the antisymmetric mode for streaking (Fig. 3). The experimental setup is otherwise identical.

The electron beam then passes through a sector magnet spectrometer and hits a microchannel plate detector where its energy and deflection spectra are analyzed with 100 eV and 0.36 mrad resolution, respectively. Roughly 2500 electrons are averaged to create one data frame.

Figure 2(a) shows a simulation of the two-stage net acceleration experiment for $e_1 = 58$ MeV/m using a symplectic tracking code based on DLATrack6D [24]. Both stages are operated symmetrically, the injection phase $\omega\Delta t$ is linearly varied, and the energy spectrum is monitored. Figure 2(b) shows the experimentally measured

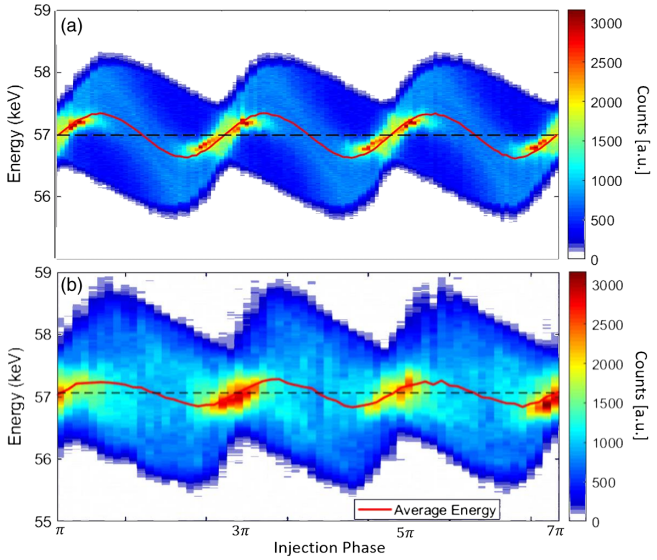

FIG. 2. (a) A two-stage accelerator simulation where the injection phase is linearly varied. $e_1 = 58$ MeV/m. The net energy gain is 350 eV, and the peak energy modulation is slightly over 1 keV. (b) The measured spectrogram for $e_1 = 58 \pm 5$ MeV/m. The net energy gain is 200 ± 10 eV, and the peak energy modulation is 1.3 keV.

spectrogram. Accurate e_1 measurement in the bunching stage is desirable, but was impeded by the presence of the second stage. e_1 in the second stage was measured to be 58 ± 5 MeV/m, and e_1 in both stages assumed to be the same. The simulated peak energy modulation is slightly over 1 keV, and the measured peak modulation is 1.3 keV, indicating that the measurement of $e_1 = 58 \pm 5$ MeV/m slightly underestimates the true e_1. However, the measured net acceleration (200 ± 10 eV) is smaller than the simulated net acceleration (350 eV). The main error source is likely to be dual-drive phase error (see the Supplemental Material [27]).

The features present in simulation are well reproduced by the experiment, and the sinusoidal variation of net energy gain is clear evidence of both microbunching and coherent control of the pulse train injection phase. Net energy gain is sharply limited by the evolution of the microbunches through the second stage—without a particle-capture mechanism, the large energy spread produced by the buncher causes the microbunches to "wash out" during acceleration. This can be significantly improved by the scheme proposed in [32], which can produce equally short microbunches with sufficiently small energy spread for injection into a monoenergetic DLA device.

By tuning the second stage to the antisymmetric mode, a streaking measurement of the microbunch duration was made by linearly varying the injection phase $\omega\Delta t$ while monitoring the deflection spectrum. e_1 was measured by measuring the energy gain in the symmetric mode of the second stage. At the optimum bunching condition, e_1 was

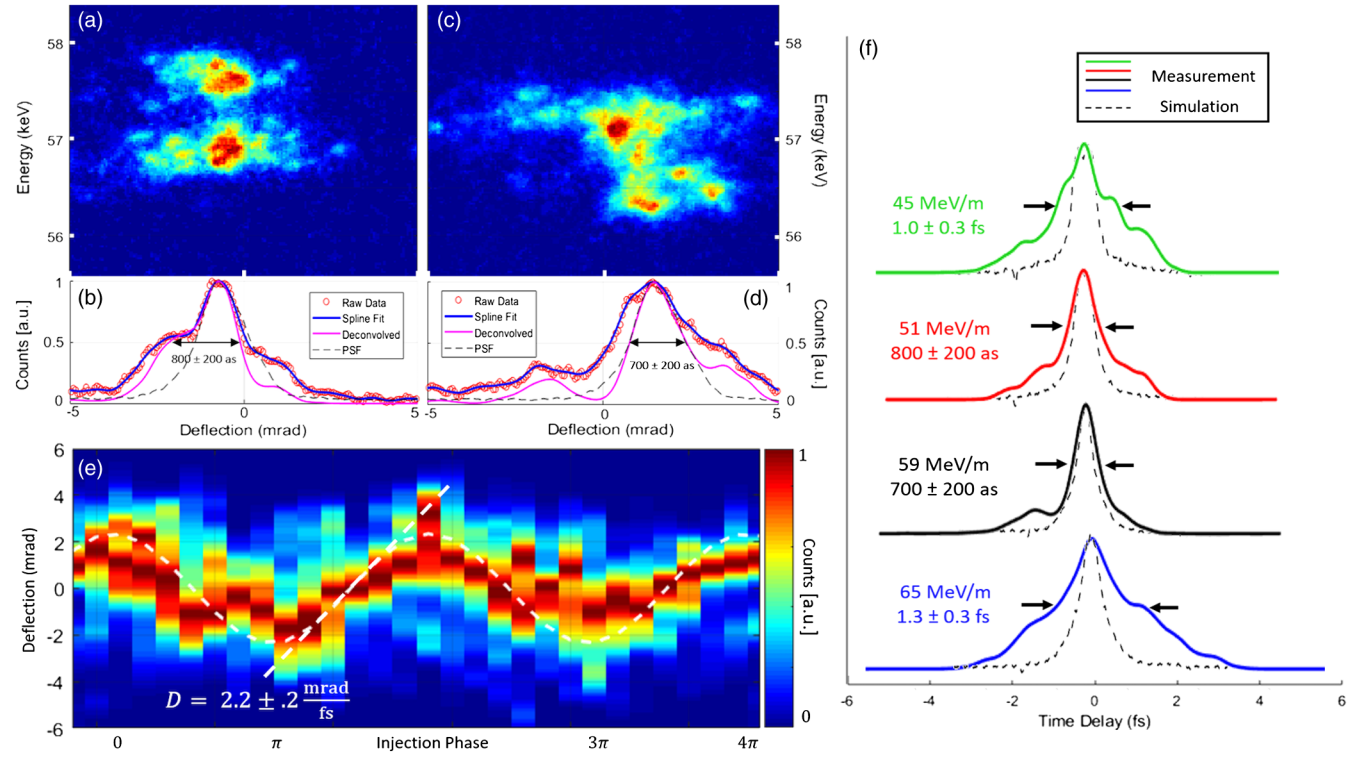

FIG. 3. (a) An MCP image of a streaked, microbunched pulse train taken from (e), showing the characteristic double-horns energy spectrum. (b) The spline fit of the deflection spectrum with the point-spread function (PSF). Their deconvolution yields the bunch temporal profile. (c) Another representative bunch from (e). (d) Its spline fit, PSF, and recovered profile. (e) A measured deflectogram as injection phase $\omega\Delta t$ is varied from 0 to 4π. e_1 is measured in the second stage to be 59 ± 5 MeV/m. The electron bunch is deflected by a total of 5 mrad over 1/2 optical cycle. The streaking speed $D = 2.2 \pm 0.2$ mrad/fs. (f) The simulated, recovered microbunch profiles (from DLATrack6D), are overlaid with the measured, averaged profiles as a function of e_1. The measured e_1 values and mean FWHM are listed next to the measured traces.

measured to be 59 ± 5 MeV/m. In this condition, 5 mrad of total deflection was observed over 1/2 optical period [Fig. 3(e)], however, this is roughly half of the value predicted by Eq. (3) using the measured e_1 value. The relative weakness of the antisymmetric mode is partially attributable to dual-drive phase error, however, 3D effects and low dual-pillar reflectivity may also play a role (see the Supplemental Material [27]).

The amplitude of the deflectogram shown in Fig. 3(e) yields a streaking speed $D = 2.2 \pm 0.2$ mrad/fs. Selected images of microbunched pulse trains from Fig. 3(e) are displayed in Figs. 3(a) and 3(c), along with their temporal profiles [Figs. 3(b) and 3(d)] after Lucy-Richardson deconvolution [33,34] with the unstreaked bunch profile (PSF). Figure 3(a) shows a clear double-horn energy spectrum characteristic of an energy modulator, and the temporal correlation of the two energy lobes, indicating microbunching. The electrons are contained within a fraction of the optical cycle corresponding to 800 ± 200 as FWHM [Fig. 3(b)] and 700 ± 200 as FWHM [Fig. 3(d)].

Figure 3(f) shows measurements of microbunch durations vs e_1. Streaking speeds for each e_1 are calculated from deflectograms analogous to Fig. 3(e), and range between 2.0 and 2.8($\pm$0.2) mrad/fs. All recovered microbunch temporal profiles within the deflectogram linear region (50% streaking amplitude) are clustered by a kernel density estimation (KDE) [35,36] algorithm, producing an average bunch duration and standard error for each cluster. The temporal profiles within each cluster are then averaged, and the minimum-duration cluster averages are shown in Fig. 3(f). Because bunch profiles are taken from all zero-crossing regions of the deflectogram, their temporal orientation (i.e., leading vs lagging edge) is not preserved after averaging, resulting in an artificial symmetrization of the bunch profile which accurately reflects the microbunch FWHM, but not the true temporal profile as in Figs. 3(b) and 3(d).

A trend is visible in Fig. 3(f)—the bunch duration is minimized as e_1 approaches the matched value (60 MeV/m), though the difference in microbunch duration between $e_1 = 59 \pm 5$ MeV/m and 51 ± 5 MeV/m is not statistically significant. The structures began to damage at higher e_1, corresponding to ~50 nJ laser pulses (~8 (mJ/cm^2) peak fluence).

The minimum resolvable bunch duration is determined by the minimum measurable broadening of the deflection spectrum, approximately 200 as for $D = 2.2\pm$ 0.2 mrad/fs. The measurement uncertainty is primarily

limited by shot noise and dual-drive laser timing jitter—these produce a standard error in measurement between 200 and 300 as, depending on the data run. Better phase stability and more electron current would significantly improve the standard error (see the Supplemental Material [27] for a discussion of measurement resolution and measurement noise).

This work demonstrates an injector prototype for a DLA composed of two dual-drive, dual-pillar stages. We demonstrate the creation of microbunched pulse trains with microbunch durations of 700 ± 200 as from a macrobunch 500 ± 100 fs in duration, and their net acceleration by 200 eV. By tuning the optical mode in the structure, we also characterize the microbunch duration with a direct streaking measurement, whose resolution is estimated to be 200 as, which is on par with the state-of-the-art for direct time-domain measurements of electron bunches.

The primary limitation of this DLA injector prototype is the energy spread produced by the bunching stage. The energy modulation necessary for μm-scale temporal focal lengths is of order 100 eV, and thus the bunch washes out after a very short distance. For bunch injection into an Alternating-Phase-Focusing (APF) DLA [32] or high-gradient DLA [1], the injector must produce a bunch with ultrashort temporal duration and small energy spread that fits inside the "accelerating bucket" in phase space. An APF DLA has longitudinal acceptance of order 10^{-13} eV s [32], which corresponds to roughly 500 eV in 300 as. A silicon APF injector is capable of producing such a beam, and this work constitutes the first step towards its realization.

The authors wish to acknowledge the entire ACHIP collaboration for their support and guidance, as well as the staff from the Stanford Nanofabrication Facility (SNF) and Stanford Nanofabrication Shared Facilities (SNSF), supported by the National Science Foundation under Grant No. ECCS-1542152. The authors also wish to acknowledge helpful discussions with R. J. England. This work is funded by the Gordon and Betty Moore Foundation (GBMF4744). U. N. additionally acknowledges funding by the German Federal Ministry of Education and Research (Grant No. FKZ: 05K16RDB).

Note added.—Similar results are reported by other members of the ACHIP collaboration in the companion Letter [37].

[1] D. Cesar, S. Custodio, J. Maxson, P. Musumeci, X. Shen, E. Threlkeld, R. J. England, A. Hanuka, I. V. Makasyuk, E. A. Peralta, K. P. Wootton, and Z. Wu, Commun. Phys. **1**, 46 (2018).
[2] K. P. Wootton *et al.*, Proc. IPAC **4744**, 2520 (2017).
[3] R. J. England *et al.*, Rev. Mod. Phys. **86**, 1337 (2014).
[4] S. Kuschel, D. Hollatz, T. Heinemann, O. Karger, M. B. Schwab, D. Ullmann, A. Knetsch, A. Seidel, C. Rödel, M. Yeung, M. Leier, A. Blinne, H. Ding, T. Kurz, D. J. Corvan, A. Sävert, S. Karsch, M. C. Kaluza, B. Hidding, and M. Zepf, Phys. Rev. Accel. Beams **19**, 071301 (2016).
[5] P. McIntosh, R. Akre, R. Boyce, P. Emma, A. Hill, and C. Rago, in *Proceedings of the IEEE Particle Accelerator Conference* (IEEE, 2005), Vol. 2005, pp. 2753–2755.
[6] D. M. Villeneuve, Contemp. Phys. **59**, 47 (2018).
[7] F. Calegari, G. Sansone, S. Stagira, C. Vozzi, and M. Nisoli, J. Phys. B: At., Mol. Opt. Phys. **49**, 062001 (2016).
[8] K. E. Priebe, C. Rathje, S. V. Yalunin, T. Hohage, A. Feist, S. Schäfer, and C. Ropers, Nat. Photonics **11**, 793 (2017).
[9] M. V. Tsarev and P. Baum, New J. Phys. **20**, 033002 (2018).
[10] A. Feist, N. Bach, N. Rubiano da Silva, T. Danz, M. Möller, K. E. Priebe, T. Domröse, J. G. Gatzmann, S. Rost, J. Schauss, S. Strauch, R. Bormann, M. Sivis, S. Schäfer, and C. Ropers, Ultramicroscopy **176**, 63 (2017).
[11] O. Lundh, C. Rechatin, J. Lim, V. Malka, and J. Faure, Phys. Rev. Lett. **110**, 065005 (2013).
[12] M. Chergui and A. H. Zewail, ChemPhysChem **10**, 28 (2009).
[13] A. H. Zewail, Annu. Rev. Phys. Chem. **57**, 65 (2006).
[14] X. Wang and Y. Li, Chin. Phys. B **27**, 076102 (2018).
[15] H. L. Andrews, C. H. Boulware, C. A. Brau, and J. D. Jarvis, Phys. Rev. ST Accel. Beams **8**, 110702 (2005).
[16] F. Lemery, P. Piot, G. Amatuni, P. Boonpornprasert, Y. Chen, J. Good, B. Grigoryan, M. Groß, M. Krasilinikov, O. Lishilin, G. Loisch, A. Oppelt, S. Philipp, H. Qian, Y. Renier, F. Stephan, and I. Zagorodnov, Phys. Rev. Lett. **122**, 044801 (2019).
[17] C. M. Sears, E. Colby, R. Ischebeck, C. McGuinness, J. Nelson, R. Noble, R. H. Siemann, J. Spencer, D. Walz, T. Plettner, and R. L. Byer, Phys. Rev. ST Accel. Beams **11**, 061301 (2008).
[18] S. Di Mitri and M. Venturini, Velocity bunching & more on magnetic-chicane bunch compression, U.S. Particle Accelerator School, http://uspas.fnal.gov/materials/13CSU/Velocity_Bunching.pdf (retrieved 2013).
[19] U. Niedermayer, O. Boine-Frankenheim, and T. Egenolf, J. Phys. Conf. Ser. **874**, 012041 (2017).
[20] C. Kealhofer, W. Schneider, D. Ehberger, A. Ryabov, F. Krausz, and P. Baum, Science **352**, 429 (2016).
[21] P. Eckle, M. Smolarski, P. Schlup, J. Biegert, A. Staudte, M. Schöffler, H. G. Muller, R. Dörner, and U. Keller, Nat. Phys. **4**, 565 (2008).
[22] J. Itatani, F. Quéré, G. L. Yudin, M. Y. Ivanov, F. Krausz, and P. B. Corkum, Phys. Rev. Lett. **88**, 173903 (2002).
[23] Y. Morimoto and P. Baum, Nat. Phys. **14**, 252 (2018).
[24] U. Niedermayer, T. Egenolf, and O. Boine-Frankenheim, Phys. Rev. Accel. Beams **20**, 111302 (2017).
[25] U. Niedermayer *et al.*, IJMPA, 10.18429/JACoW-ICAP2018-MOPLG01 (2019).
[26] K. J. Leedle, D. S. Black, Y. Miao, K. E. Urbanek, A. Ceballos, H. Deng, J. S. Harris, O. Solgaard, and R. L. Byer, Opt. Lett. **43**, 2181 (2018).
[27] See the Supplemental Material at http://link.aps.org/supplemental/10.1103/PhysRevLett.123.264802 for a detailed discussion of the experimental error in the microbunch duration measurement, as well as a description of the forces inside a dual-grating structure, specifically high-

lighting a correction term proportional to the dual-pillar reflectivity which may explain discrepancies between theory and experiment. It also contains representative energy and deflection spectra from the modulator (stage 1) and streaker (stage 2) stages, operated individually and in the symmetric mode. The Supplemental Material includes Ref. [28].

[28] R. J. England, A. Ody, and Z. Huang, Report No. SLAC-PUB-17450 (SLAC, 2019).

[29] D. Nguyen, J. Lewellen, and L. Duffy, Bunch Compression—RF Linacs for High-Gain FEL, U.S. Particle Accelerator School, http://uspas.fnal.gov/materials/14UNM/E_Bunch_Compression.pdf (retrieved 2014).

[30] D. S. Black, K. J. Leedle, Y. Miao, U. Niedermayer, R. L. Byer, and O. Solgaard, Phys. Rev. Lett. **122**, 104801 (2019).

[31] A. Ceballos (to be published).

[32] U. Niedermayer, T. Egenolf, O. Boine-Frankenheim, and P. Hommelhoff, Phys. Rev. Lett. **121**, 214801 (2018).

[33] L. B. Lucy, Astron. J. **79**, 745 (1974).

[34] W. H. Richardson, J. Opt. Soc. Am. **62**, 55 (1972).

[35] E. Parzen, Ann. Math. Stat. **33**, 1065 (1962).

[36] M. Rosenblatt, Ann. Math. Stat. **27**, 832 (1956).

[37] N. Schönenberger, A. Mittelbach, P. Yousefi, J. McNeur, and P. Hommelhoff, following Letter, Phys. Rev. Lett. **123**, 264803 (2019).